



*Citation for published version:*

Farrar, LS, Zajicek, Z, Morfoot, AB, Bristow, M, Humphries, OS, Haghighirad, AA, McCollam, A, Bending, SJ & Coldea, AI 2022, 'Unconventional localization of electrons inside of a nematic electronic phase', *Proceedings of the National Academy of Sciences of the United States of America*, vol. 119, no. 43, e2200405119.  
<https://doi.org/10.1073/pnas.2200405119>

*DOI:*

[10.1073/pnas.2200405119](https://doi.org/10.1073/pnas.2200405119)

*Publication date:*

2022

*Document Version*

Peer reviewed version

[Link to publication](#)

*Publisher Rights*

CC BY

**University of Bath**

**Alternative formats**

If you require this document in an alternative format, please contact:  
[openaccess@bath.ac.uk](mailto:openaccess@bath.ac.uk)

**General rights**

Copyright and moral rights for the publications made accessible in the public portal are retained by the authors and/or other copyright owners and it is a condition of accessing publications that users recognise and abide by the legal requirements associated with these rights.

**Take down policy**

If you believe that this document breaches copyright please contact us providing details, and we will remove access to the work immediately and investigate your claim.

# Unconventional localization of electrons inside of a nematic electronic phase

Liam S. Farrar<sup>a,1</sup>, Zachary Zajicek<sup>b</sup>, Archie B. Morfoot<sup>b</sup>, Matthew Bristow<sup>b</sup>, Oliver S. Humphries<sup>b</sup>, Amir A. Haghighirad<sup>b,c</sup>, Alix McCollam<sup>d</sup>, Simon J. Bending<sup>a</sup>, and Amalia I. Coldea<sup>b,2</sup>

<sup>a</sup>Centre for Nanoscience and Nanotechnology, Department of Physics, University of Bath, Bath, BA2 7AY, United Kingdom ; <sup>b</sup>Clarendon Laboratory, Department of Physics, University of Oxford, Parks Road, Oxford OX1 3PU, UK; <sup>c</sup>Institute for Quantum Materials and Technologies, Karlsruhe Institute of Technology, 76021 Karlsruhe, Germany; <sup>d</sup>High Field Magnet Laboratory (HFML-EMFL), Radboud University, 6525 ED Nijmegen, The Netherlands

This manuscript was compiled on September 12, 2022

**The magnetotransport behaviour inside the nematic phase of bulk FeSe reveals unusual multiband effects that cannot be reconciled with a simple two-band approximation proposed by surface-sensitive spectroscopic probes. In order to understand the role played by the multiband electronic structure and the degree of two-dimensionality we have investigated the electronic properties of exfoliated flakes of FeSe by reducing their thickness. Based on magnetotransport and Hall resistivity measurements, we assess the mobility spectrum that suggests an unusual asymmetry between the mobilities of the electrons and holes with the electron carriers becoming localized inside the nematic phase. Quantum oscillations in magnetic fields up to 38 T indicate the presence of a hole-like quasiparticle with a lighter effective mass and a quantum scattering time three times shorter, as compared with bulk FeSe. The observed localization of negative charge carriers by reducing dimensionality can be driven by orbitally-dependent correlation effects, enhanced interband spin-fluctuations or a Lifshitz-like transition which affect mainly the electron bands. The electronic localization leads to a fragile two-dimensional superconductivity in thin flakes of FeSe, in contrast to the two-dimensional high- $T_c$  induced with electron doping via dosing or using a suitable interface.**

Magnetotransport | Superconductivity | Quantum oscillations

Among different classes of unconventional superconductors, iron-based systems display rich physics due to their multiband structure and the competition between different electronic interactions (1). Iron-chalcogenides are among the most strongly correlated iron-based superconductors and, due to the large intra-atomic exchange caused by the Hund's coupling, the correlation strengths are expected to be strongly orbitally dependent (2). This orbital differentiation can lead to an orbital-selective Mott transition, or spectral weight transfer, where the band with dominant  $d_{xy}$  orbital appears more insulating while other bands with  $d_{xz}$  and  $d_{yz}$  orbital character remain metallic (1, 3). As a result, electronic and superconducting properties are likely to be influenced by these effects, as seen in orbitally-dependent band shifts in angle-resolved photoemission spectroscopy (ARPES) in iron-chalcogenides (4, 5) and orbital-dependent Cooper pairing (6).

FeSe is a candidate system in which the presence of the lower-Hubbard band establishes the important role of electronic correlations, orbital-dependent band shifts in the nematic phase and Fermi surface shrinking (7–10). The strength of these effects can be suppressed by isoelectronic substitution with sulphur (11–13). The interatomic Coulomb repulsion in FeSe can produce a strongly renormalized low-energy band structure where the van Hove singularity sits remarkably close to the Fermi level in the high-temperature electron liquid phase

(14). ARPES studies under strain suggest that in FeSe one electron pocket either is missing or the spectral weight is transferred between its two electron pockets (3, 15). Furthermore, neutron scattering suggests the coexistence of both stripe and Néel spin fluctuations with a substantial amount of spectral weight transferred towards stripe spin fluctuations inside the nematic phase (16). The lack of long-range antiferromagnetic order in FeSe has been linked to the competition between different types of magnetic order that can lead to significant magnetic frustration (17).

Transport properties of systems with orbitally-dependent correlations are predicted to display a coherence-incoherence crossover as a function of temperature (18) and, in addition, nematic iron-based superconductors are prone to anisotropic single-particle scattering enhanced by interband spin or charge fluctuations (19). In the presence of spin fluctuations, the scattering is strongly influenced by quasiparticles close to *hot spots* at Fermi surface locations where the nesting is strong (20, 21). Furthermore, the large fluctuating moments with Néel and stripe magnetic instabilities (16) are likely to strongly affect the magnetotransport behaviour. Magnetotransport studies of FeSe and FeSe<sub>1-x</sub>S<sub>x</sub> have identified a linear resistivity regime and a large magnetoresistance inside the nematic phase

## Significance Statement

Among iron-based superconductors, FeSe displays an anomalous electronic nematic state, strong electronic correlations and orbitally-dependent band shifts that can influence its superconducting pairing. Here, we report a detailed magnetotransport study of thin flakes of FeSe that reveals unconventional transport in which the hole carriers remain highly mobile, whereas the mobility of the electron carriers is low, with hardly any temperature dependence, inside the nematic phase. This suggests an unusual localization of negative charge carriers that may be caused by orbital-dependent enhanced correlations, scattering of spin fluctuations and/or a topological electronic transition. As the superconductivity is suppressed by reducing the flake thickness, it suggests that the electron pockets participate actively in the superconducting pairing. By doping, electron pockets expand and enable the high- $T_c$  superconductivity.

**Author Contributions** LF has prepared the thin flake devices. ABM, MB, LF and AIC performed experiments in Oxford. AIC, MB, ZZ and AM performed experiments in Nijmegen. AAH grew the single crystals. LF, SJB and AIC performed the data analysis. AIC and LF wrote the paper with contributions and comments from all the authors.

The authors declare no conflict of interest. This article contains supporting information online at [www.pnas.org/cgi/doi/10.1073/pnas.XXXXXXXXXX](http://www.pnas.org/cgi/doi/10.1073/pnas.XXXXXXXXXX).

<sup>2</sup>To whom correspondence should be addressed. E-mail: [amalia.coldea@physics.ox.ac.uk](mailto:amalia.coldea@physics.ox.ac.uk)

(22, 23). However, the low-field magnetotransport data in the normal state suggest that, in addition to one hole and one almost compensated electron band, the nematic phase of FeSe exhibits an additional tiny electron pocket with a high mobility and non-linear Hall coefficient (23, 24) that can also be found in the low pressure regime (25). Additionally, the amplitude of the quantum oscillations at low temperatures and high magnetic fields indicates that hole carriers are likely to be more mobile than electron bands (23), and the highly mobile holes and enhanced spin fluctuations also dominate the high- $T_c$  pressure phase of FeSe (26).

In this paper, we present a detailed magnetotransport study of exfoliated thin flakes of FeSe as compared with bulk single crystals. The mobility spectrum and a two-band model reveal that the mobility of the holes in thin flake devices is much higher than that of electrons. Electrons become localized at low temperatures, due to the enhancement of the orbitally-dependent correlations and enhanced anisotropic scattering in two-dimensional devices. From quantum oscillations we find that the size of the extremal hole orbit is smaller and the effective mass of the hole band is lighter than in bulk. In the low-temperature regime, the resistivity shows a linear dependence down to the lowest temperatures but Fermi liquid behaviour is restored in the cleanest flake, where quantum oscillations are present. While the thinner devices could be sensitive to increased impurity and surface scattering, the reduction in  $T_c$  in thin flakes is directly correlated with the suppression of the nematic phase and the localization of electron carriers.

## Results

**Transport properties of thin flakes of FeSe.** Fig. 1(a) shows the temperature dependence of the normalized zero-field resistance,  $\rho(T)/\rho(300\text{K})$ , for a bulk crystal and six different thin flake devices with thicknesses in the range  $t=14\text{--}125\text{ nm}$ . Bulk FeSe undergoes a tetragonal to orthorhombic distortion at  $T_s \approx 90\text{ K}$  without any accompanying long-range magnetic order, followed by the onset of superconductivity at  $T_c \sim 9\text{ K}$  (30). These parameters in single crystals are sensitive to the growth conditions and the impurity level; the suppression of  $T_c$  is affected by the increase in the amount of disorder, as measured by the residual resistivity ratio ( $RRR$ ), which linearly correlates with the suppression of  $T_s$  (31). In thin flakes, the superconducting transition temperature,  $T_c$ , is already lowered from the bulk single crystal value to  $7.2\text{ K}$  for a  $t = 125\text{ nm}$  device, decreasing further to  $3.6\text{ K}$  for a  $t = 14\text{ nm}$  device, as reported previously (27). The suppression of superconductivity in the  $t = 125\text{ nm}$  device occurs despite the high residual resistance ratio of  $RRR \sim 32$ , which is similar to bulk crystals from the same batch (22). In thinner flakes, the  $RRR$  value falls as a function of decreasing thickness, reducing to  $5.5$  in the  $t = 14\text{ nm}$  device as shown in Fig. S4(c) in the SI Appendix (32), being similar to the effect of impurity scattering by Cu doping in FeSe (33, 34). Similarly, the emergence of the nematic phase at  $T_s$ , which results in significant in-plane distortion of the Fermi surface and orbitally-dependent band shifts (10), becomes smeared and less defined for thinner flakes. Fig. 1(b) shows the variation of  $T_s$  and  $T_c$  as a function of inverse thickness ( $1/t$ ) for different devices, revealing that both are suppressed for thinner flakes; interestingly, we find a linear dependence between  $T_s$  and  $T_c$ , as found in Cu-substituted

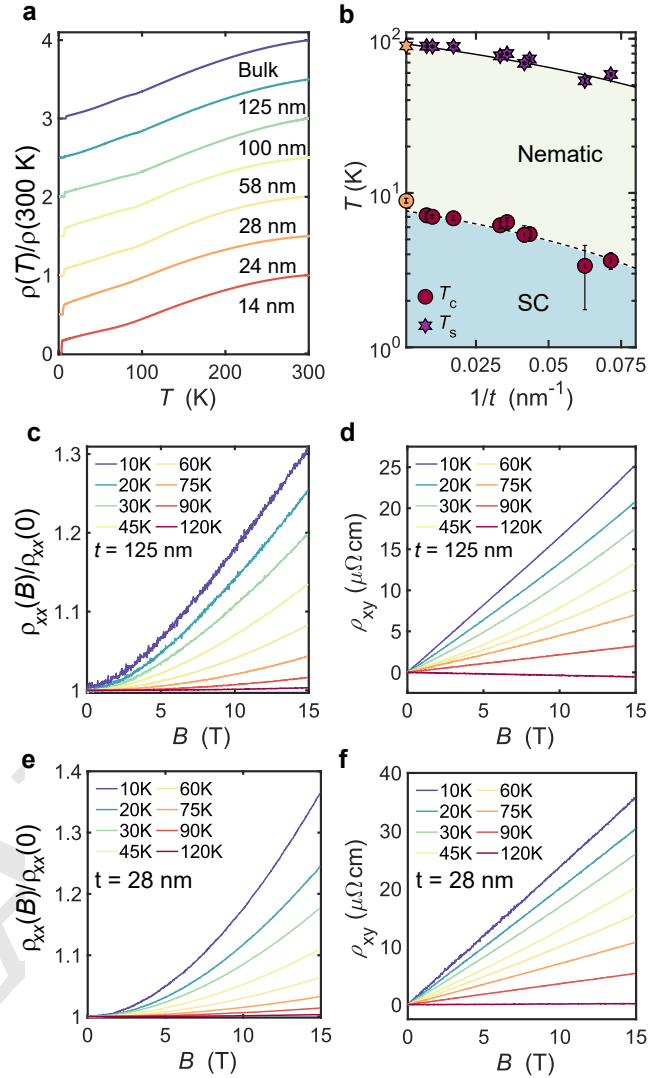


**Fig. 1.** Magnetotransport of thin flakes of FeSe. (a) Temperature dependence of the normalised zero-field resistance  $\rho(T)/\rho(300\text{K})$  for a bulk crystal and different thin flake devices ( $t = 14\text{--}125\text{ nm}$ ). Data are vertically offset and this panel is updated with new data from Ref. (27). (b) Inverse thickness  $t$  dependence of the superconducting transition temperature,  $T_c$ , and the structural transition temperature,  $T_s$ . Bulk values are shown on the left with light orange symbols. The dashed line is a fit to the Cooper model and the solid line is a guide to the eye for the changes in  $T_s$  with the thickness  $t$  (28, 29). (c-f) The magnetic field dependence of the longitudinal and transverse components of the resistivity,  $\rho_{xx}$  and  $\rho_{xy}$ , at different constant temperatures for two devices with  $t=125$  and  $t = 28\text{ nm}$ .

FeSe (34) (see Fig. S4(b) in SI Appendix (32)). As these two parameters are correlated and are suppressed as the  $RRR$  ratio is reduced, it suggests that the two-dimensional confinement, enhanced fluctuations and surface impurity scattering, play an important role in the suppression of  $T_c$  in thin flakes of FeSe (27).

**Low-field magnetotransport behaviour.** Figs. 1(c-f) show the field dependence of the longitudinal magnetoresistance normalized by the zero-field value,  $\rho_{xx}(B)/\rho_{xx}(0)$ , and the Hall resistivity,  $\rho_{xy}$ , for two different devices with  $t = 125$  and  $28\text{ nm}$ , respectively. FeSe is a multi-band stoichiometric compound in which charge compensation requires that  $n = n_e = n_h$ . At high temperatures in the tetragonal phase, the magneto-

transport properties of bulk FeSe can be accurately described using a compensated two-band model, as detailed in the SI Appendix (32). This model corresponds to a hole pocket at the Brillouin zone centre and an electron pocket at the corner of the Brillouin zone (23). This two-band picture also describes the high temperature magnetotransport behaviour of thin flakes whereby the magnetoresistance does not saturate and  $\rho_{xy}$  shows a linear dependence on magnetic field (see Fig. S5 in the SI Appendix (32)).

Inside the nematic phase (below 75 K), the Hall component  $\rho_{xy}$  of bulk crystals of FeSe displays non-linear behaviour in magnetic field and a negative slope (23) and a deviation from the compensated two-band behaviour, whereas all thin flake devices display a positive Hall component in magnetic field (see also Fig. S5 in the SI Appendix (32)). To visualize the differences between the bulk and thin flakes, Fig. 2(c) shows the temperature dependence of the Hall coefficient,  $R_H = \rho_{xy}/B$  in low magnetic fields ( $B < 1$  T). All the thin flake devices have a positive Hall coefficient below  $T_s$  suggesting that the transport behaviour becomes increasingly dominated by the hole-like carriers. We detect a local maximum in  $R_H$  around 65 K for the  $t = 125$  nm, which is close to the temperature at which the Hall coefficient of bulk FeSe (23) and also the resistivity anisotropy under strain changes sign (35). These striking changes in transport behaviour could signify the development of anisotropic scattering effects inside the nematic phase which can be enhanced by lowering the temperature and reducing the thickness. The  $\rho_{xy}(B)$  component deviates from a linear dependence in magnetic field in the same temperature regime (see corresponding derivatives in Fig. S5 in the SI Appendix (32)). However, linear dependence is detected at the lowest temperatures, in the regime of isotropic scattering caused mainly by impurities, and at the highest temperatures, where electron-phonon scattering becomes important, similar to other reports on thin flakes (36). Overall, the behaviour of the Hall coefficient in thin flakes of FeSe is in stark contrast to bulk FeSe, in which  $R_H$  becomes negative below the nematic transition, as seen in Fig. 2c.

**Mobility spectrum.** To analyse in detail the origin of the changes inside the nematic phase, we perform a mobility-spectrum analysis of the magnetotransport data (Fig. 2). This approach has previously been successful in characterising the transport behaviour of bulk FeSe (24) and other multi-band systems (37). The modelling is based on the methodology detailed in Ref. (38), which eliminates the need for making *a priori* assumptions on the transport parameters in a multicarrier system and describes the mobility spectrum,  $s(\mu) = e\mu n(\mu)$ , with the negative electron charge assigned to a negative value of mobility. Fig. 2(a) shows the evolution of the normalised mobility spectrum  $s(\mu)/s(\mu_{max})$  for the  $t = 125$  nm device as a function of temperature. The height of  $s(\mu)$  could be linked to the variation of the number of carriers,  $n(\mu)$ , whereas the width of the peak of  $s(\mu)$  relates to a distribution of relaxation times and the magnetic field resolution, such that  $\mu B < 1$  (38) (see Fig. S9 in the SI Appendix (32)). As a function of temperature, the mobility of positive charge carriers increases strongly with decreasing temperature reaching  $\mu_h \sim 1200 \text{ cm}^2 \text{ V}^{-1} \text{ s}^{-1}$  at 10 K. On the other hand, the electron mobility has a much weaker increase with decreasing temperature, and below 50 K the corresponding mobility peak position only shifts slightly from  $|\mu_{e1}| \sim 300(50) \text{ cm}^2 \text{ V}^{-1} \text{ s}^{-1}$ . As the mobility of the holes

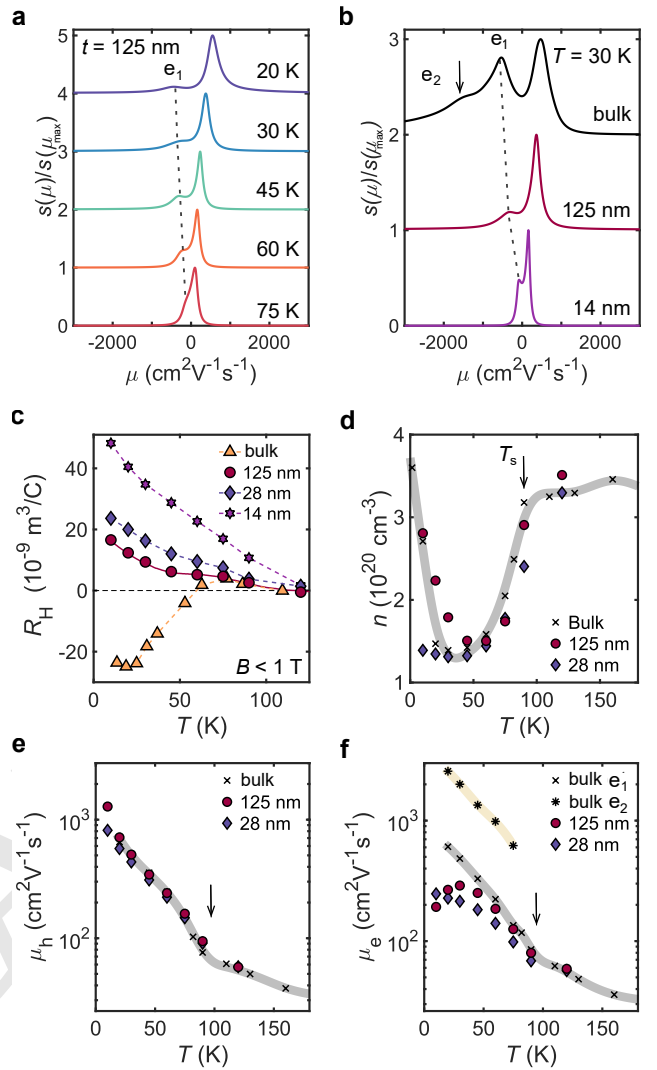


**Fig. 2.** The changes in the carrier mobilities with temperature. (a) Temperature dependence of the normalized mobility spectra to the maximum value  $s(\mu_{max})$  of electron-like (negative) and hole-like (positive) carriers for a  $t = 125$  nm device. (b) A comparison of the normalized mobility spectra to the to the maximum value  $s(\mu_{max})$  for a bulk crystal and different thin flake devices of FeSe at  $T = 30$  K. The spectra are vertically offset for clarity. Dotted line shows the mobilities of the electron charge carrier  $e_1$  and the arrow indicates the highly mobile electron,  $e_2$ , found only in the bulk. (c) The temperature dependence of the low field Hall coefficient  $R_H$  (extracted for  $B < 1$  T) for a bulk FeSe crystal and three thin flake devices. (d) Temperature dependence of the carrier density extracted using a compensated two-carrier model  $n = n_e + n_h$  (see SI Appendix (32)). Temperature dependence of carrier mobilities for (e) the hole-like carriers,  $\mu_h$ , and (f) electron-like carriers,  $\mu_e$ , for various samples. The data points for the bulk single crystals of FeSe and the three-carrier model parameters are from Ref. (23) and the solid lines are guides to the eye. The vertical arrows indicate the position of  $T_s$ .

is larger than that of electrons, it explains the positive sign of the Hall coefficient in thin flakes, shown in Fig. 2(c).

Next, we compare the mobility spectrum of two different flake devices with those of the bulk crystal at 30 K, as shown in Fig. 2(b). The bulk mobility spectrum has a complex shape for the electron-like charge carriers, that could indicate the presence of an additional highly mobile electron band,  $e_2$ , (or the existence of sharp changes in curvature of the Fermi surface for electron-like flower shape pockets in Fig. 4(b)), besides the mobility shoulder corresponding to the high carrier

density electron band,  $e_1$ . This behaviour is in agreement with a previous report indicating a broad mobility spectrum for electrons, with the highly mobile carriers assigned as ultra-fast Dirac-like carriers in bulk FeSe (24). This highly mobile carrier,  $e_2$ , is not visible in any of the thin flakes, even for the 125 nm flake which has a similar value of  $RRR$  to that of the bulk. This suggests a high sensitivity of the electronic structure, in particular the electron pockets, to reduced interlayer coupling and enhanced two-dimensional confinement. Fig. 2(b) also shows that the mobilities of both electron and hole carriers in general decrease with the thickness of the flakes and reduced  $RRR$  ratio (see Fig. S4(c) in SI Appendix (32)). In the case of the thinnest flake with  $t = 14$  nm, both the electron  $e_1$  and hole mobilities have been drastically reduced, as compared to the bulk crystal ( $|\mu_{e1}| = 80$  and  $\mu_h = 160$   $\text{cm}^2\text{V}^{-1}\text{s}^{-1}$  at 30 K).

To provide quantitative insights into the behaviour of the charge carriers in the thin flakes, we simultaneously fit the two resistivity components,  $\rho_{xx}$  and  $\rho_{xy}$ , to the compensated two-band model using the values from the mobility spectrum as starting parameters. Figs. 2(d-f) show the temperature dependence of the carrier density  $n = n_h = n_e$ , and the field-independent mobilities  $\mu_h$  and  $\mu_e$ , compared with those for the bulk single crystals of FeSe (23). At high temperatures, the extracted values for  $n$  are similar to those of bulk samples, which show a relatively constant carrier density of  $n \approx 3 - 4 \times 10^{20}$   $\text{cm}^{-3}$ . Unexpectedly, the carrier density shows a marked reduction of more than a factor of 2 at 45 K, before rapidly increasing back to the high temperature value below 10 K. This drop in carrier density below  $T_s$  cannot be reconciled with the expectation that the Fermi surface pockets should only deform but not change size inside the nematic phase, in the absence of any spin-density wave order. This anomalous behaviour may be caused by the onset of strongly anisotropic scattering at the Fermi surfaces below  $T_s$  (11), arising from the presence of strong spin fluctuations (39), as different parts of the Fermi surfaces that are nested by the antiferromagnetic ordering vector will experience a dramatic increase in the scattering rate (40). The calculated drop in the effective carrier density,  $n$ , in the absence of any change in the Fermi surface volume, could be a manifestation of strongly anisotropic scattering inside the nematic phase or that some of the charge carriers become more localized and do not contribute to transport behaviour. However,  $n$  recovers its value in the low temperature limit for  $t=125$  nm flake where the isotropic impurity scattering dominates, similar to the bulk behaviour (23).

Figs. 2(e,f) show the extracted mobilities from the two-band analysis which confirms the striking difference in the mobility behaviour of the two types of charge carriers ( $\mu_h$  and  $\mu_{e1}$ ). For all the measured thin flake devices, the hole mobilities are much larger than those of electrons, exhibiting a similar temperature dependence to that of the bulk band. There is a slightly decreased mobility of  $\mu_h = 810$   $\text{cm}^2\text{V}^{-1}\text{s}^{-1}$  at  $T = 10$  K for the  $t = 28$  nm sample, attributed to the increasing importance of surface scattering due to the increasing surface-to-volume ratio in thinner samples as well as the reduction of the residual resistivity ratio due to other extrinsic effects (additional scattering from charged centres in the  $\text{SiO}_2$  substrate). In contrast to the behaviour of the holes, the electron mobility of thin flakes displays a much weaker temperature dependence that deviates significantly from the

bulk  $e_1$  value. Actually, the electron mobility plateaus in thin flake samples at low temperatures, as is clearly seen in the mobility data of Fig. 2(f). The contrasting behaviour of the mobilities of the holes and electrons is unexpected and correlates with the suppression of superconductivity in thin flakes in two-dimensions. This behaviour in FeSe is different from that found in iron-pnictides where electrons are often more mobile than holes (41). Our findings are in broad agreement with the results of terahertz spectroscopy in FeSe thin films that detect that the scattering time of the hole carrier becomes substantially longer than that of the electron at lower temperatures (42). Highly mobile hole carriers were also found in the high- $T_c$  phase of bulk FeSe under pressure (43).

**High-field magnetotransport.** Figs. 3(a) and (b) show the magnetotransport behaviour of a  $t = 58$  nm flake in high magnetic fields up to 37.5 T. The Hall resistivity is observed to be strictly linear in magnetic field as expected for a perfectly compensated two-band system. However, the longitudinal magnetoresistance exhibits an unconventional  $B^{1.6}$  dependence for different devices (Fig. S6 and Fig. S7 in the SI Appendix (32)), similar to that found in bulk FeSe at high magnetic fields (22). Fig. 3(c) shows in-plane magnetotransport studies that are not affected by orbital effects, as the current and magnetic field are parallel to each other; the linear high field extrapolation is used to access the low temperature normal resistivity, as shown in Fig. 3(d). We find that the low temperature resistivity has a linear temperature dependence to the lowest temperatures for most of the measured flakes (Figs. S7(f) and S8(b) in the SI Appendix (32)), except for the one which displays quantum oscillations, as shown in Fig. 3(d). A crossover transition to the Fermi liquid behaviour occurs below 5 K for  $t = 58$  nm, but this crossover is highly sensitive to the degree of impurity scattering, as found in  $\text{FeSe}_{1-x}\text{S}_x$  (22) and Cu-substituted FeSe (34). Linear dependence at the lowest temperature is found for a flake with  $t = 100$  nm (Fig. S7(f) in the SI Appendix (32)) and it describes the resistivity behaviour below 50 K for both orthorhombic directions in another flake in Fig. S8 in the SI Appendix (32). This behaviour is often a hallmark of scattering by spin fluctuations in the vicinity of an antiferromagnetic critical point (44, 45).

At the lowest temperatures we have detected quantum oscillations for one of the flakes with  $t = 58$  nm, both in  $\rho_{xx}$  and  $\rho_{xy}$  components (Fig. 3(a) and (b)), with the amplitude of the signal in the Hall component being stronger. Fig. 3(e) shows quantum oscillations in the  $\rho_{xy}$  component having an amplitude a factor of 10 smaller than bulk single crystals (23). The fast Fourier transform (FFT) spectra help to identify the extremal areas of the Fermi surface pockets normal to the applied magnetic field,  $A_{ki}$ , via the Onsager relation,  $F_i = A_{ki}\hbar/(2\pi e)$  (46). The low temperature experimental Fermi surface of FeSe is composed of one warped cylindrical hole band at  $\Gamma$  with oscillation frequencies  $\beta$  ( $k_z = 0$ ,  $F = 164$  T) and  $\delta$  ( $k_z = \pi/c$ ,  $F = 664$  T), and potentially two warped cylindrical electron Fermi surfaces that are located at the corners of the Brillouin zone (see Fig. 3(f) and Fig. 4(b)) (7, 10, 47). Fig. 3(f) shows the dominant oscillation frequency of the  $t = 58$  nm thin flake is 595 T, which is likely to correspond to the largest orbit at the  $Z$  point of the hole band  $\delta$ . The signal from the hole bands was also found to be dominant in the  $\rho_{xy}$  for bulk crystals (23). The observed reduction

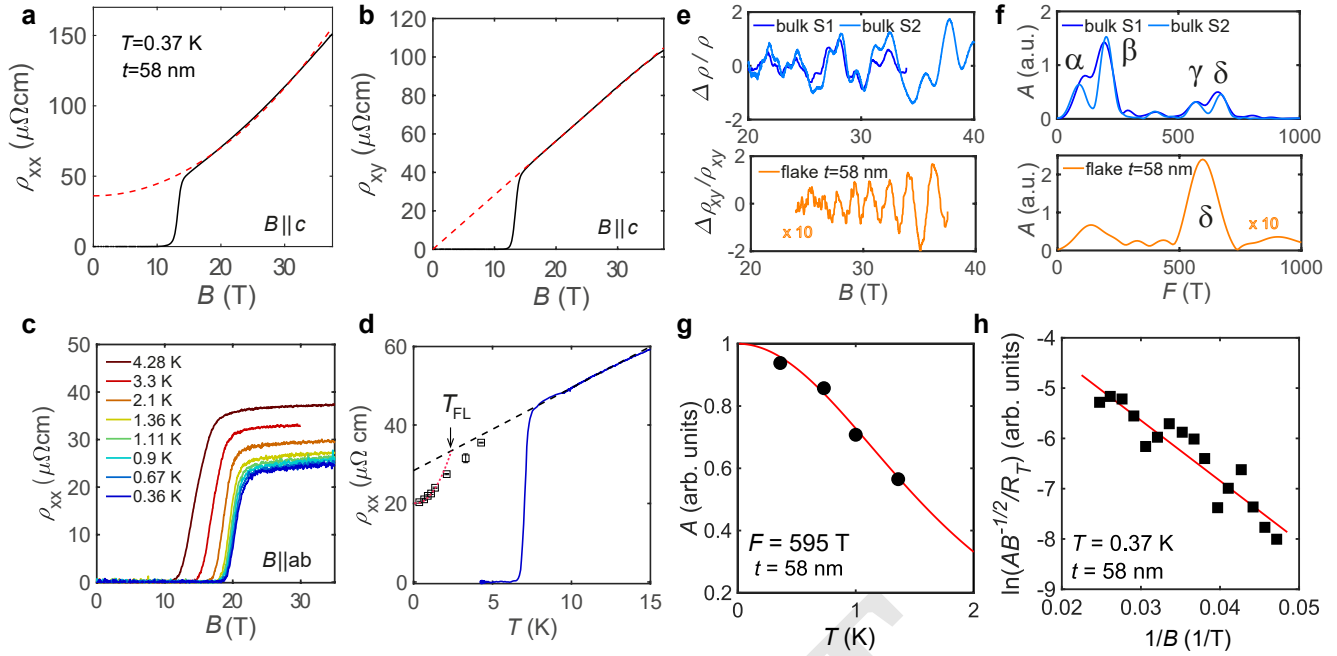


**Fig. 3.** High-field magnetotransport and quantum oscillations in a thin flake device of FeSe. (a) Longitudinal resistivity and (b) Hall resistivity as a function of  $B$  for a  $t = 58$  nm flake at  $T = 0.37$  K. The dashed lines are fits to a two-band model with  $\mu_h = 1017 \text{ cm}^2\text{V}^{-1}\text{s}^{-1}$  and  $\mu_e = 231 \text{ cm}^2\text{V}^{-1}\text{s}^{-1}$ . (c) In-plane resistivity as a function of magnetic field at different fixed temperatures. (d) Low temperature zero-field resistivity together with extrapolated data from panel (c) assuming that  $\rho_{xx}$  is linearly dependent on  $B$  in (c) for  $H \parallel (ab)$  (open squares). The dashed line is a linear fit to the data. The arrow indicates the crossover to a Fermi liquid  $T^2$  behaviour below  $T_{FL}$  (dotted line). (e) Quantum oscillations,  $\Delta\rho_{xy}/\rho_{xy}$ , of the  $t = 58$  nm flake and two bulk single crystals in  $\rho_{xy}$  for S1 and  $\rho_{xx}$  for S2. (f) The corresponding FFT spectra from (e) for the flake and the bulk sample. The amplitude of the oscillations of the  $t = 58$  nm flake is multiplied by a factor of 10 in (e) and (f). (g) The temperature dependence of the oscillation amplitude for the  $t = 58$  nm flake. A Lifshitz-Kosevich (LK) fit (solid line) yields an effective carrier mass of  $m_{\text{eff}} = 3.1(2)m_e$  for the hole pocket  $\delta$ , located at the centre of the Brillouin zone. (h) The corresponding Dingle plot for the estimation of the slope which gives  $T_D = 4.5(4)$  K.

in the size of the extremal area of the Fermi surface of the thin flake could suggest a reduction of  $k_z$  warping due to an increase in the degree of two-dimensionality in the thin flakes. The cyclotron-averaged effective masses of the quasiparticles extracted from the temperature dependence of the amplitude of the quantum oscillations in Fig. 3(g) (using raw data from Fig. S6(a) in the SI Appendix (32)) is found to be  $\sim 3.1(2)m_e$ , slightly lighter than  $\sim 4.5(1)m_e$ , found for the bulk  $\delta$  pocket (7, 47).

**Scattering.** In order to quantify how the amplitude of quantum oscillations is affected by impurity scattering, we estimate the Dingle temperature,  $T_D$ , as shown in Fig. 3(h) and detailed in the SI Appendix (32) and Ref. (48). The slope gives a  $T_D = 4.5(4)$  K which corresponds to a quantum mean free path of  $\ell_q \sim 140 \text{ \AA}$  for the  $t = 58$  nm device. The quantum scattering time,  $\tau_q = \hbar/(2\pi k_B T_D)$ , corresponds to the time taken to fully randomise the linear momentum of an electron; it is found to be  $\tau_q = 0.27(2)$  ps, corresponding to a quantum hole mobility of  $\mu_q \sim 158 \text{ cm}^2/\text{Vs}$ . This quantum scattering time for the  $\delta$  hole pocket is almost a factor of 3 shorter than in bulk FeSe, where  $\tau_q = 0.7(1)$  ps, as shown in Fig. S2 in the SI Appendix (32). This could indicate an increase in the impurity and surface scattering in this thin flake, as its  $RRR$  is smaller than the bulk (Fig. 4(b)). Furthermore, the classical mobility from the two-band model yields a value close to  $\mu_h = 1017 \text{ cm}^2\text{V}^{-1}\text{s}^{-1}$ , corresponding to a classical scattering time of  $\tau_h \sim 1.8$  ps, using the effective mass from quantum oscillations of  $3.1(2)m_e$ . The large difference (a factor of 6) between the two scattering occurs due to the sensitivity of the

quantum mobility to both small and large angle scattering events, while the transport mobility is mainly dominated by large angle scattering (49).

## Discussion

The unconventional behaviour in magnetotransport of thin flakes of FeSe suggests the strong sensitivity of the quasiparticle scattering and Fermi surface inside the nematic phase (Fig. 4(a)). Below  $T_s$ , there are significant changes in the shape of the Fermi surface caused by orbitally-band dependent shifts (10, 13). The 3D hole pocket, centered at the Z point, is pushed below the Fermi level due to orbital ordering, and the in-plane pockets become strongly elongated (Fig. 4(a)). This change of the in-plane anisotropy is not expected to change the carrier density,  $n$ , by a factor of 2 inside the nematic phase (10, 13), which normally occurs when the Fermi surface undergoes a significant reconstruction, as for  $\text{BaFe}_2\text{As}_2$  in the presence of the SDW phase (56). Thus, the drastic changes in the Hall coefficient and carrier densities of FeSe, imply either that certain charge carriers inside the nematic phase scatter much more, or get redistributed onto more localized  $d_{xy}$  bands, and thus do not participate in conduction. Additionally, the small quasi-two dimensional Fermi surface pockets could also suffer topological changes inside the nematic phase (Fig. 4(b)), as found in thin films of FeSe (54) or induced by small applied strain (52).

The Hall coefficient, in the low field limit, is very sensitive to the momentum-dependent scattering and the curvature of the Fermi surface. The Fermi surface topology and the changes

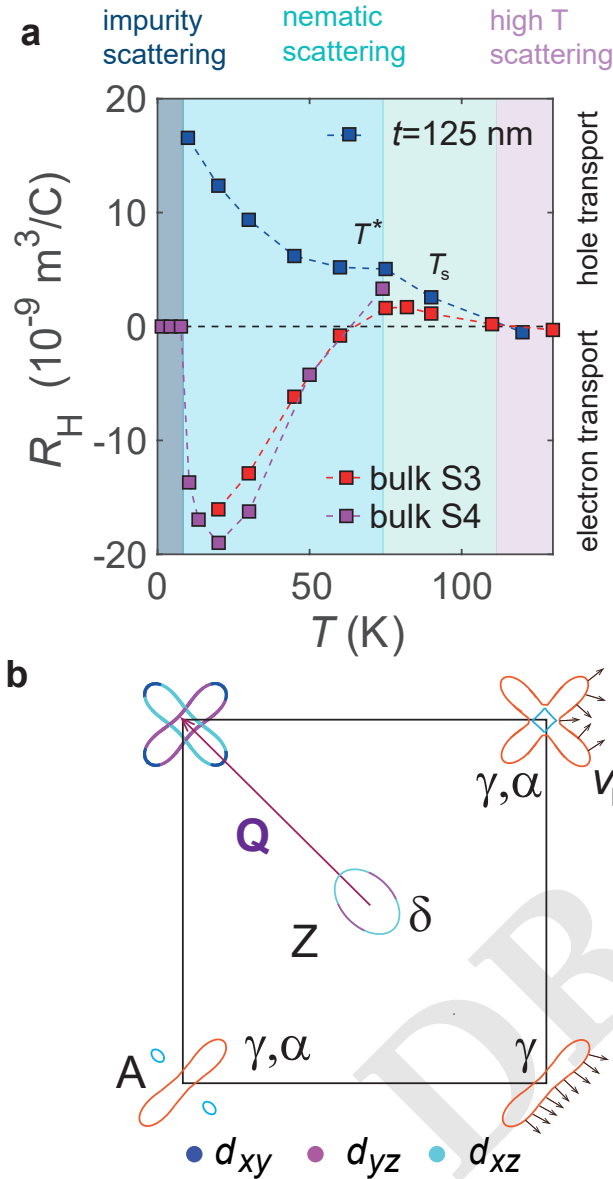


**Fig. 4.** Anomalous transport of FeSe. (a) The temperature dependence of the Hall coefficient in bulk single crystals (S3 from Ref. (23) and S4 from (22)) as compared with a clean  $t = 125$  nm flake of FeSe, with similar  $RRR \sim 32$  value (Fig. S4(c) in the SI Appendix (32)). The potential different regimes of scattering are illustrated by different coloured regions, as detailed in Ref. (40). Inside the nematic phase, the orbital ordering and spin-orbit coupling can generate sizable in-plane anisotropy in susceptibility below  $T^*$  (50). (b) Schematic Fermi surface of FeSe at low temperatures based on quantum oscillations for  $k_z = \pi/c$  (13, 51). The electron orbits in the corner of the Brillouin zone reflect different representations induced by orbital ordering, spin-orbit coupling and strain (13, 52–54), from two electron pockets (top corners) to a single peanut pocket (bottom right) or a single peanut with two small pockets (bottom left). The small arrows indicate the variation of the Fermi velocity when the magnetic field is normal to the plane of the pocket that could generate electron and hole contributions to the Hall effect (55). The dominant orbital character of the Fermi surface is shown in the top left corner. Hot spots can be generated at the crossing point between elliptical electron pockets (40).

in curvature from convex to concave around a pocket, leads to the variation of the scattering path vector,  $\mathbf{l}_k = \mathbf{v}_F \tau_k$ . The enclosed area swept by the  $\mathbf{l}_k$  vector, as  $\mathbf{k}$  moves around the Fermi surface, will change sign, which directly affects the sign

of the Hall conductivity (55) (see Fig. S10 in the SI Appendix (32)). The Fermi surface of FeSe at low temperatures has an elliptical hole pocket and one or two electron pockets, as represented in Fig. 4(b). The difference between the Hall coefficient of bulk and thin flakes in Fig. 4(a) could be linked to a topological change of the Fermi surface, induced by orbital ordering (13); this could transform a flower-shape pocket, with convex and concave curvatures and negative Hall coefficient, into an elongated ellipse in thin flakes, with a convex curvature that gives a positive Hall coefficient (Fig. 4(b) and Fig. S10 in the SI Appendix (32)). The small electron pocket  $e_2$  pocket of the bulk ( $\alpha$  pocket) is absent in the mobility spectrum of thin flakes of FeSe. As the inner electron band is located very close to the Fermi level, it is highly sensitive to small changes in energy ( $\sim 3$ meV), upon reducing the thickness of the flakes, and under applied uniaxial strain. This pocket already disappears in thin films of FeSe (54) (Fig. 4(b)), due to the orbital and momentum-dependent energy splitting at the M point that is larger for thin films ( $\sim 70$  meV) (54) than in bulk ( $\sim 50$  meV) (10). Furthermore, ARPES studies of bulk FeSe under strain, that probe the surface and bulk layers up to  $\sim 10$  Å (57), usually detects a single electron pocket in the corner of the Brillouin zone that can be induced by applied strain (52, 53) (Fig. 4(b)).

The strong disparity between the hole and electron mobilities behaviour (up to a factor of 6 at 10 K), and the observation of the rather temperature-independent mobility of the electron carriers below 50 K could imply an enhancement of the orbitally-averaged effective masses and/or orbitally-dependent scattering that affect mainly the electron pockets. The proximity to a van-Hove singularity caused by orbitally-dependent shifts in FeSe can also amplify the small angle scattering processes for the electron pockets. Using the low temperature mobility values of electrons of  $\mu_e = 231$  cm<sup>2</sup>/(Vs) and  $\tau \sim 1.8$  ps, from the two-band model (Fig. 3(a) and (b)) one can estimate the effective mass to be  $\sim 13 m_e$  for the  $t = 58$  nm flake. This value is much larger than the orbitally-averaged effective mass of  $\sim 7 m_e$  of the electron pocket  $\gamma$  for bulk crystals (Fig. 4(b))(7) and it would be difficult to detect experimentally in quantum oscillations (Fig. 3(f)). Assuming that the effective masses of heavy electrons are the same for the bulk and thin flakes, then the changes in mobilities between electron and hole carriers could reflect an anisotropy in scattering (classical scattering time being  $\sim 0.9$  ps for electrons and 1.8 ps for holes). Interestingly, the effective mass extracted from ARPES studies is much smaller,  $\sim 1 m_e$  for a single momentum direction (7, 13) and it can be enhanced in thin films and flakes of FeSe up to  $\sim 4 m_e$  both using K-dosing of FeSe (58) and ionic liquid gating (59). Orbitally-dependent band shifts and renormalizations were detected previously in FeSe, with the dominant  $d_{xy}$  hole band being the most renormalized by a factor of 8 as compared with a factor 2.5-3.5 for the  $d_{xz}$  and  $d_{yz}$  orbitals (2, 7). Interestingly, the part of the electron pockets with  $d_{xy}$  character can become completely incoherent (Fig. 4(b)) and hard to detect in surface-sensitive experiments (60). Alternatively, there is an exchange of  $d_{xy}$  spectral weight from one electron pockets towards the other electron pocket, as suggested by recent ARPES studies under strain (3). Furthermore, the orbitally-dependent pairing between electron and hole pockets was detected from surface studies using STM measurements of FeSe (60, 61).

The Hall coefficient  $R_H$  of FeSe increases with decreasing temperature and has an inflection point at  $T^* \sim 75$  K, for both bulk and thin flakes, as shown in Fig. 4(a). On cooling  $R_H$  starts deviating and  $n$  is significantly reduced inside the nematic phase, as if there is a loss of available charge carriers. (Fig. 2(d)). At the temperature  $T^*$ , applied strain has the weakest effect on resistivity and the transport anisotropy changes sign (35). The change in resistivity anisotropy coincides also with the temperature at which a large anisotropy develops in the local spin susceptibility (62). Thus, the anisotropy of the local magnetism affects the quasiparticle scattering and the coherent coupling between local spins and itinerant electrons. The sign of the Hall coefficient is always positive in thin flakes but negative in the bulk below  $\sim 60$  K, despite having similar  $RRR$  values. The Hall coefficient is also positive in Cu-substituted FeSe with large impurity scattering (33, 34) and in thin films of  $\text{FeSe}_{1-x}\text{S}_x$  (63). Furthermore, it also becomes positive by using the isoelectronic sulphur substitution in single crystals of  $\text{FeSe}_{1-x}\text{S}_x$  (for  $x > 0.11$ ) (22, 64, 65), due to subtle changes in the band structure and spin-fluctuation scattering (13, 22). At lowest temperature, there is a crossover from inelastic to impurity-dominated scattering, when the  $n$  value normally recovers to the high-temperature tetragonal case (Fig. 4(a)). The very large increase in  $R_H$  observed in the thinnest  $t = 14$  nm flake resembles the behaviour of thin films of FeSe with lower  $RRR$  values (59). Recently, it was shown theoretically that the impurity scattering in FeSe can give rise to anisotropic scattering and anisotropy in resistivity (66). Furthermore, a strong role of orbital-differentiation on the temperature dependence of  $R_H$  has also been found in other systems, like  $\text{Sr}_2\text{RuO}_4$  (67) and  $\text{FeCrAs}$  (68).

Despite the lack of long-range magnetic order in FeSe, there is a large energy range of magnetic fluctuations due to the relatively small spin-fluctuation bandwidth together with the low-carrier density (16). In zero-magnetic field in thin flakes, we detect a linear resistivity below 50 K in most flakes, (Fig. S8(b) in the SI Appendix (32)) except in the cleanest samples in which a crossover to Fermi liquid behaviour occurs, Fig. 3(d). The linear resistivity occurs for both orthorhombic directions consistent with scattering by critical antiferromagnetic fluctuations in the presence of disorder which is strongly enhanced at *hot spots* on the Fermi surface where the nesting is perfect (Fig. 4(b)) (19, 21, 44). In the presence of spin fluctuations, the quasiparticle currents dressed by vertex corrections acquire the character of the majority carriers and lead to a larger absolute Hall coefficient with a marked temperature dependence (69). Additionally, the localization of electrons could be enhanced by spin-fluctuations that affect interband scattering between elliptical electron pockets, like the Néel-type fluctuations, as compared with interband stripe order fluctuations between holes and electrons (Fig. 4(b)). Short-range, weak Néel fluctuations strongly suppress the  $s_{\pm}$  superconducting state and can lead to a low- $T_c$   $d$ -wave state (70).

## Concluding Remarks

In summary, we have performed a detailed study of electronic transport of high quality FeSe thin flakes and identify an unusual localization effect of negative charge carriers inside the nematic phase. This disparity between hole and electrons emphasizes the anomalous transport inside the nematic phase,

driven by the subtle interplay between the changes in the electronic structure of a multi-band system and the unusual scattering processes induced by orbital-dependent enhanced correlations and/or anisotropic spin fluctuations. The two-dimensional confinement of thin flakes affects the mobility of the electron-like carriers significantly but also plays a role in their superconductivity which is suppressed. These effects emphasize the complexity and sensitivity of the electron pockets in FeSe-based systems which are involved in the stabilization of a two-dimensional high- $T_c$  superconductivity via electron doping induced by interfacial effects or dosing.

## Materials and Methods

**Experimental details.** Thin FeSe flakes were mechanically exfoliated from high quality single crystals onto silicone elastomer polydimethylsiloxane (PDMS) stamps. Flakes of suitable geometry and thickness were then transferred onto Si/SiO<sub>2</sub> (300 nm oxide) substrates with pre-patterned Au-contacts using a dry transfer set-up housed in a nitrogen glovebox with an oxygen and moisture content  $< 1$  ppm. To minimise environmental exposure, a capping layer of thin ( $\sim 20$  nm) hexagonal boron nitride (h-BN) was transferred on top of the FeSe flake. The thickness of each sample was measured using an atomic force microscope (AFM) after all magnetotransport measurements had been performed. Magnetotransport measurements at temperatures down to 2 K and magnetic fields up to 16 T were performed using a Quantum Design Physical Property Measurement system (PPMS) in Oxford, with high field measurements performed at the High Field Magnet Laboratory in Nijmegen (up to 37.5 T) in a Helium-3 cryostat. The magnetoresistance and Hall resistivity contributions were separated by symmetrizing and antisymmetrizing the data obtained in positive and negative magnetic fields. The non-ideal flake and contact geometries were accounted for by numerically evaluating the resistance to resistivity conversion factors. Details of these calculations are provided in the Supplementary Information (Fig. S1 in the SI Appendix (32)).

**Data availability.** The data that support the findings of this study will be made available through the open access data archive at the University of Oxford (ORA) at <https://doi.org/10.5287/bodleian:X5GgyEj1O>.

**ACKNOWLEDGMENTS.** We would like to thank Steve Simon and Siddharth Parameswar for useful discussions and Roemer Hinlopen for the development of the software used to estimate the scattering path length for an arbitrary Fermi surface. The research was funded by the Oxford Centre for Applied Superconductivity (CFAS) at Oxford University. We also acknowledge financial support of the John Fell Fund of the Oxford University. This work was partly supported by EPSRC (EP/I004475/1, EP/I017836/1). LF was supported by the Bath/Bristol Centre for Doctoral Training in Condensed Matter Physics, under the EPSRC (UK) Grant No. EP/L015544. Part of this work was supported by HFML-RU/FOM, members of the European Magnetic Field Laboratory (EMFL) and by EPSRC (UK) via its membership to the EMFL (EP/N01085X/1). AAH acknowledges the financial support of the Oxford Quantum Materials Platform Grant (EP/M020517/1). Z.Z. acknowledges financial support from the EPSRC studentship (EP/N509711/1 and EP/R513295/1) AIC acknowledges an EPSRC Career Acceleration Fellowship (EP/I004475/1).

1. Rafael M. Fernandes, Amalia I. Coldea, Hong Ding, Ian R. Fisher, P. J. Hirschfeld, and Gabriel Kotliar. Iron pnictides and chalcogenides: a new paradigm for superconductivity. *Nature*, 601 (7891):35–44, 2022. ISSN 1476-4687. . URL <https://doi.org/10.1038/s41586-021-04073-2>.
2. Z. P. Yin, K. Haule, and G. Kotliar. Kinetic frustration and the nature of the magnetic and paramagnetic states in iron pnictides and iron chalcogenides. *Nat. Mater.*, 10(12):932–5, dec 2011. ISSN 1476-1122. . URL <http://www.ncbi.nlm.nih.gov/pubmed/21927004>.
3. C. Cai, T. T. Han, Z. G. Wang, L. Chen, Y. D. Wang, Z. M. Xin, M. W. Ma, Yuan Li, and Y. Zhang. Anomalous spectral weight transfer in the nematic state of iron-selenide superconductor. *Chinese Physics B*, 29(7):077401, aug 2020. . URL <https://doi.org/10.1088/1674-1056/ab90ec>.
4. Ming Yi, Zhongkai Liu, Yan Zhang, Rong Yu, Jianxin Zhu, James Lee, Rob Moore, Felix Schmitt, Wei Li, Scott Riggs, Jiun-Haw Chu, Bing Lv, Jin Hu, Makoto Hashimoto, Sung-Kwan Mo, Zahid Hussain, Zhiqiang Mao, Ching-Wu Chu, Ian Fisher, Qimiao Si, Zhi-Xun Shen, and



- Donghui Lu. Observation of universal strong orbital-dependent correlation effects in iron chalcogenides. *Nat. Comm.*, 6:7777, 2015. .
5. Z. K. Liu, M. Yi, Y. Zhang, J. Hu, R. Yu, J.-X. Zhu, R.-H. He, Y. L. Chen, M. Hashimoto, R. G. Moore, S.-K. Mo, Z. Hussain, Q. Si, Z. Q. Mao, D. H. Lu, and Z.-X. Shen. Experimental observation of incoherent-coherent crossover and orbital-dependent band renormalization in iron chalcogenide superconductors. *Phys. Rev. B*, 92:235138, Dec 2015. . URL <https://link.aps.org/doi/10.1103/PhysRevB.92.235138>.
  6. P. O. Sprau, A. Kostin, A. Kreisel, A. E. Böhmer, V. Taufour, P. C. Canfield, S. Mukherjee, P. J. Hirschfeld, B. M. Andersen, and J. C. Séamus Davis. Discovery of orbital-selective Cooper pairing in FeSe. *Science*, 357(6346):75–80, 2017. ISSN 0036-8075. . URL <https://science.sciencemag.org/content/357/6346/75>.
  7. M. D. Watson, T. K. Kim, A. A. Haghighirad, N. R. Davies, A. McCollam, A. Narayanan, S. F. Blake, Y. L. Chen, S. Ghannadzadeh, A. J. Schofield, M. Hoesch, C. Meingast, T. Wolf, and A. I. Coldea. Emergence of the nematic electronic state in FeSe. *Phys. Rev. B*, 91:155106, 2015. ISSN 1098-0121. . URL <http://link.aps.org/doi/10.1103/PhysRevB.91.155106>.
  8. Laura Fanfarillo, Joseph Mansart, Pierre Toulemonde, Hervé Cercellier, Patrick Le Fèvre, François Bertran, Belen Valenzuela, Lara Benfatto, and Véronique Brout. Orbital-dependent Fermi surface shrinking as a fingerprint of nematicity in FeSe. *Phys. Rev. B*, 94:155138, Oct 2016. . URL <https://link.aps.org/doi/10.1103/PhysRevB.94.155138>.
  9. Matthew D. Watson, Steffen Backes, Amir A. Haghighirad, Moritz Hoesch, Timur K. Kim, Amalia I. Coldea, and Roser Valentí. Formation of Hubbard-like bands as a fingerprint of strong electron-electron interactions in FeSe. *Phys. Rev. B*, 95:081106, Feb 2017. . URL <http://link.aps.org/doi/10.1103/PhysRevB.95.081106>.
  10. A. I. Coldea and M. D. Watson. The key ingredients of the electronic structure of FeSe. *Annu. Rev. Cond. Matt. Phys.*, 9, 2018. .
  11. M. D. Watson, T. K. Kim, A. A. Haghighirad, S. F. Blake, N. R. Davies, M. Hoesch, T. Wolf, and A. I. Coldea. Suppression of orbital ordering by chemical pressure in  $\text{FeSe}_{1-x}\text{S}_x$ . *Phys. Rev. B*, 92:121108, 2015. ISSN 1098-0121. . URL <http://link.aps.org/doi/10.1103/PhysRevB.92.121108>.
  12. P. Reiss, M. D. Watson, T. K. Kim, A. A. Haghighirad, D. N. Woodruff, M. Bruma, S. J. Clarke, and A. I. Coldea. Suppression of electronic correlations by chemical pressure from FeSe to FeS. *Phys. Rev. B*, 96:121103, Sep 2017. . URL <https://link.aps.org/doi/10.1103/PhysRevB.96.121103>.
  13. Amalia I. Coldea. Electronic Nematic States Tuned by Isoelectronic Substitution in Bulk  $\text{FeSe}_{1-x}\text{S}_x$ . *Frontiers in Physics*, 8:528, 2021. . URL <https://www.frontiersin.org/article/10.3389/fphy.2020.594500>.
  14. K. Jiang, J. Hu, H. Ding, and Z. Wang. Interatomic Coulomb interaction and electron nematic bond order in FeSe. *Phys. Rev. B*, 93:115138, 2016. ISSN 2469-9950. . URL <http://journals.aps.org/prb/abstract/10.1103/PhysRevB.93.115138>.
  15. Matthew D. Watson, Amir A. Haghighirad, Luke C. Rhodes, Moritz Hoesch, and Timur K. Kim. Electronic anisotropies revealed by detwinned angle-resolved photo-emission spectroscopy measurements of FeSe. *New Journal of Physics*, 19(10):103021, 2017. . URL <https://doi.org/10.1088%2F1367-2630%2Faa8a04>.
  16. Q. Wang, Y. Shen, B. Pan, Y. Hao, M. Ma, F. Zhou, P. Steffens, K. Schmalzl, T. R. Forrest, M. Abdel-Hafiez, X. Chen, D. A. Chareev, A. N. Vasiliev, P. Bourges, Y. Sidis, H. Cao, and J. Zhao. Strong interplay between stripe spin fluctuations, nematicity and superconductivity in FeSe. *Nat. Mater.*, 15(2):159, feb 2016. ISSN 1476-1122. URL <http://dx.doi.org/10.1038/nmat449210.1038/nmat449210><http://www.nature.com/nmat/journal/v15/n2/abs/nmat4492.html#supplementary-information>.
  17. J. K. Glasbrenner, I. I. Mazin, H. O. Jeschke, P. J. Hirschfeld, R. M. Fernandes, and R. Valentí. Effect of magnetic frustration on nematicity and superconductivity in iron chalcogenides. *Nature Physics*, 11(11):953, 2015. URL <http://www.nature.com/nphys/journal/v11/n11/full/nphys3434.html>.
  18. K. Haule and G. Kotliar. Coherence-incoherence crossover in the normal state of iron oxypnictides and importance of Hund's rule coupling. *New Journal of Physics*, 11(2):025021, feb 2009. . URL <https://doi.org/10.1088/1367-2630/11/2/025021>.
  19. Maxim Breitkreiz, P. M. R. Brydon, and Carsten Timm. Transport anomalies due to anisotropic interband scattering. *Phys. Rev. B*, 88:085103, Aug 2013. . URL <https://link.aps.org/doi/10.1103/PhysRevB.88.085103>.
  20. A. Rosch. Magnetotransport in nearly antiferromagnetic metals. *Phys. Rev. B*, 62:4945–4962, Aug 2000. . URL <https://link.aps.org/doi/10.1103/PhysRevB.62.4945>.
  21. A. E. Koshelev. Magnetotransport of multiple-band nearly antiferromagnetic metals due to hot-spot scattering. *Phys. Rev. B*, 94:125154, Sep 2016. . URL <https://link.aps.org/doi/10.1103/PhysRevB.94.125154>.
  22. M. Bristow, P. Reiss, A. A. Haghighirad, Z. Zajicek, S. J. Singh, T. Wolf, D. Graf, W. Knafo, A. McCollam, and A. I. Coldea. Anomalous high-magnetic field electronic state of the nematic superconductors  $\text{FeSe}_{1-x}\text{S}_x$ . *Phys. Research*, 2:013309, Mar 2020. . URL <https://link.aps.org/doi/10.1103/PhysRevResearch.2.013309>.
  23. M. D. Watson, T. Yamashita, S. Kasahara, W. Knafo, M. Nardone, J. Béard, F. Hardy, A. McCollam, A. Narayanan, S. F. Blake, T. Wolf, A. A. Haghighirad, C. Meingast, A. J. Schofield, H. v. Löhneysen, Y. Matsuda, A. I. Coldea, and T. Shibauchi. Dichotomy between the Hole and Electron Behavior in Multiband Superconductor FeSe Probed by Ultra-high Magnetic Fields. *Phys. Rev. Lett.*, 115:027006, 2015. ISSN 0031-9007. . URL <http://link.aps.org/doi/10.1103/PhysRevLett.115.027006>.
  24. K. K. Huynh, Y. Tanabe, T. Urata, H. Oguro, S. Heguri, K. Watanabe, and K. Tanigaki. Electric transport of a single-crystal iron chalcogenide FeSe superconductor: Evidence of symmetry-breakdown nematicity and additional ultrafast Dirac cone-like carriers. *Phys. Rev. B*, 90:144516, Oct 2014. . URL <http://link.aps.org/doi/10.1103/PhysRevB.90.144516>.
  25. Taichi Terashima, Naoki Kikugawa, Andhika Kiswandhi, David Graf, Eun-Sang Choi, James S. Brooks, Shigeru Kasahara, Tatsuya Watashige, Yuji Matsuda, Takasada Shibauchi, Thomas Wolf, Anna E. Böhmer, Frédéric Hardy, Christoph Meingast, Hilbert v. Löhneysen, and Shinya Uji. Fermi surface reconstruction in FeSe under high pressure. *Phys. Rev. B*, 93:094505, Mar 2016. . URL <http://link.aps.org/doi/10.1103/PhysRevB.93.094505>.
  26. J. P. Sun, K. Matsuura, G. Z. Ye, Y. Mizukami, M. Shimozawa, K. Matsubayashi, M. Ya-mashita, T. Watashige, S. Kasahara, Y. Matsuda, J.-Q. Yan, B. C. Sales, Y. Uwatoko, J.-G. Cheng, and T. Shibauchi. Dome-shaped magnetic order competing with high-temperature superconductivity at high pressures in FeSe. *Nat. Commun.*, 7:12146, 2016. .
  27. Liam S Farrar, Matthew Bristow, Amir A Haghighirad, Alix McCollam, Simon J Bending, and Amalia I Coldea. Suppression of superconductivity and enhanced critical field anisotropy in thin flakes of FeSe. *npj Quantum Materials*, 5(1):29, 2020. ISSN 2397-4648. . URL <https://doi.org/10.1038/s41535-020-0227-3>.
  28. Leon N. Cooper. Superconductivity in the neighborhood of metallic contacts. *Phys. Rev. Lett.*, 6:689–690, Jun 1961. . URL <https://link.aps.org/doi/10.1103/PhysRevLett.6.689>.
  29. J. Simonin. Surface term in the superconductive Ginzburg-Landau free energy: Application to thin films. *Phys. Rev. B*, 33:7830–7832, Jun 1986. . URL <https://link.aps.org/doi/10.1103/PhysRevB.33.7830>.
  30. A. E. Böhmer, F. Hardy, F. Eilers, D. Ernst, P. Adelman, P. Schweiss, T. Wolf, and C. Meingast. Lack of coupling between superconductivity and orthorhombic distortion in stoichiometric single-crystalline FeSe. *Phys. Rev. B*, 87(18):180505, may 2013. ISSN 1098-0121. . URL <http://link.aps.org/doi/10.1103/PhysRevB.87.180505>.
  31. A. E. Böhmer, V. Taufour, W. E. Straszheim, T. Wolf, and P. C. Canfield. Variation of transition temperatures and residual resistivity ratio in vapor-grown FeSe. *Phys. Rev. B*, 94:024526, Jul 2016. . URL <http://link.aps.org/doi/10.1103/PhysRevB.94.024526>.
  32. For further details consult the si appendix at <https://www.pnas.org/content/suppl/xxx>.
  33. Chunsheng Gong, Shanshan Sun, Shaohua Wang, and Hechang Lei. Normal and superconducting state properties of Cu-doped FeSe single crystals. *Phys. Rev. B*, 103:174510, May 2021. . URL <https://link.aps.org/doi/10.1103/PhysRevB.103.174510>.
  34. Z. Zajicek, S. J. Singh, H. Jones, P. Reiss, M. Bristow, A. Martin, A. Gower, A. McCollam, and A. I. Coldea. Drastic effect of impurity scattering on the electronic and superconducting properties of Cu-doped FeSe. *Phys. Rev. B*, 105:115130, Mar 2022. . URL <https://link.aps.org/doi/10.1103/PhysRevB.105.115130>.
  35. Michele Ghini, Matthew Bristow, Joseph C. A. Prentice, Samuel Sutherland, Samuele Sanna, A. A. Haghighirad, and A. I. Coldea. Strain tuning of nematicity and superconductivity in single crystals of FeSe. *Phys. Rev. B*, 103:205139, May 2021. . URL <https://link.aps.org/doi/10.1103/PhysRevB.103.205139>.
  36. B. Lei, J. H. Cui, Z. J. Xiang, C. Shang, N. Z. Wang, G. J. Ye, X. G. Luo, T. Wu, Z. Sun, and X. H. Chen. Evolution of High-Temperature Superconductivity from a Low- $T_c$  Phase Tuned by Carrier Concentration in FeSe Thin Flakes. *Phys. Rev. Lett.*, 116:077002, Feb 2016. . URL <https://link.aps.org/doi/10.1103/PhysRevLett.116.077002>.
  37. Haijun Zhao, Wencong Li, Yue Chen, Chunqiang Xu, Bin Li, Weidong Luo, Dong Qian, and Zhixiang Shi. Transport property of multi-band topological material  $\text{PtBi}_2$  studied by maximum entropy mobility spectrum analysis (MEMSA). *Scientific Reports*, 11(1):6249, 2021. ISSN 2045-2322. . URL <https://doi.org/10.1038/s41598-021-85364-6>.
  38. W. A. Beck and J. R. Anderson. Determination of electrical transport properties using a novel magnetic field-dependent hall technique. *Journal of Applied Physics*, 62(2):541–554, 1987. . URL <https://doi.org/10.1063/1.339780>.
  39. P. Wiecek, K. Rana, A. E. Böhmer, Y. Lee, S. L. Bud'ko, P. C. Canfield, and Y. Furukawa. Persistent correlation between superconductivity and antiferromagnetic fluctuations near a nematic quantum critical point in  $\text{FeSe}_{1-x}\text{S}_x$ . *Phys. Rev. B*, 98:020507, Jul 2018. . URL <https://link.aps.org/doi/10.1103/PhysRevB.98.020507>.
  40. Maxim Breitkreiz, P. M. R. Brydon, and Carsten Timm. Transport in multiband systems with hot spots on the Fermi surface: Forward-scattering corrections. *Phys. Rev. B*, 89:245106, Jun 2014. . URL <https://link.aps.org/doi/10.1103/PhysRevB.89.245106>.
  41. S. Kasahara, K. Hashimoto, H. Ikeda, T. Terashima, Y. Matsuda, and T. Shibauchi. Contrasts in electron correlations and inelastic scattering between  $\text{LiFeP}$  and  $\text{LiFeAs}$  revealed by charge transport. *Phys. Rev. B*, 85:060503, Feb 2012. . URL <https://link.aps.org/doi/10.1103/PhysRevB.85.060503>.
  42. Naotaka Yoshikawa, Masayuki Takayama, Naoki Shikama, Tomoya Ishikawa, Fuyuki Nabeshima, Atsutaka Maeda, and Ryo Shimano. Charge carrier dynamics of FeSe thin film investigated by terahertz magneto-optical spectroscopy. *Phys. Rev. B*, 100:035110, Jul 2019. . URL <https://link.aps.org/doi/10.1103/PhysRevB.100.035110>.
  43. J. P. Sun, G. Z. Ye, P. Shahi, J.-Q. Yan, K. Matsuura, H. Kontani, G. M. Zhang, Q. Zhou, B. C. Sales, T. Shibauchi, Y. Uwatoko, D. J. Singh, and J.-G. Cheng. High- $T_c$  Superconductivity in FeSe at High Pressure: Dominant Hole Carriers and Enhanced Spin Fluctuations. *Phys. Rev. Lett.*, 118:147004, Apr 2017. . URL <https://link.aps.org/doi/10.1103/PhysRevLett.118.147004>.
  44. A. Rosch. Interplay of disorder and spin fluctuations in the resistivity near a quantum critical point. *Phys. Rev. Lett.*, 82:4280–4283, May 1999. . URL <https://link.aps.org/doi/10.1103/PhysRevLett.82.4280>.
  45. S. Kasahara, T. Shibauchi, K. Hashimoto, K. Ikada, S. Tonegawa, R. Okazaki, H. Shishido, H. Ikeda, H. Takeya, K. Hirata, T. Terashima, and Y. Matsuda. Evolution from non-Fermi- to Fermi-liquid transport via isovalent doping in  $\text{BaFe}_2(\text{As}_{1-x}\text{P}_x)_2$  superconductors. *Phys. Rev. B*, 81:184519, May 2010. . URL <https://link.aps.org/doi/10.1103/PhysRevB.81.184519>.
  46. D. Shoenberg. *Magnetic Oscillations in Metals*. Cambridge University Press, Cambridge, 1984.
  47. Taichi Terashima, Naoki Kikugawa, Andhika Kiswandhi, Eun-Sang Choi, James S. Brooks, Shigeru Kasahara, Tatsuya Watashige, Hiroaki Ikeda, Takasada Shibauchi, Yuji Matsuda, Thomas Wolf, Anna E. Böhmer, Frédéric Hardy, Christoph Meingast, Hilbert v. Löhneysen, Michi-to Suzuki, Rytarou Arita, and Shinya Uji. Anomalous Fermi surface in FeSe seen by Shubnikov-de Haas oscillation measurements. *Phys. Rev. B*, 90:144517, Oct 2014. . URL <http://link.aps.org/doi/10.1103/PhysRevB.90.144517>.
  48. Antony Carrington. Quantum oscillation studies of the Fermi surface of iron-pnictide superconductors. *Reports Prog. Phys.*, 74(12):124507, dec 2011. ISSN 0034-4885. . URL <http://stacks.iop.org/0034-4885/74/i=12/a=124507>.
  49. A. Narayanan, M. D. Watson, S. F. Blake, N. Bruyant, L. Drigo, Y. L. Chen, D. Prabhakaran, B. Yan, C. Felser, T. Kong, P. C. Canfield, and A. I. Coldea. Linear Magnetoresistance Caused by Mobility Fluctuations in  $n$ -Doped  $\text{Cd}_3\text{As}_2$ . *Phys. Rev. Lett.*, 114:117201, Mar 2015. . URL <https://link.aps.org/doi/10.1103/PhysRevLett.114.117201>.
  50. J. Li, B. Lei, D. Zhao, L. P. Nie, D. W. Song, L. X. Zheng, S. J. Li, B. L. Kang, X. G. Luo, T. Wu,

- and X. H. Chen. Spin-orbital-intertwined nematic state in fese. *Phys. Rev. X*, 10:011034, Feb 2020. . URL <https://link.aps.org/doi/10.1103/PhysRevX.10.011034>.
51. A. I. Coldea, S. F. Blake, S. Kasahara, A. A. Haghighirad, M. D. Watson, W. Knafo, E. S. Choi, A. McCollam, P. Reiss, T. Yamashita, M. Bruma, S. Speller, Y. Matsuda, T. Wolf, T. Shibauchi, and A. J. Schofield. Evolution of the low-temperature Fermi surface of superconducting  $\text{FeSe}_{1-x}\text{S}_x$  across a nematic phase transition. *npj Quantum Materials*, 4:2, 2019. . URL <https://www.nature.com/articles/s41535-018-0141-0>.
  52. Matthew D. Watson, Amir A. Haghighirad, Luke C. Rhodes, Moritz Hoesch, and Timur K. Kim. Electronic anisotropies revealed by detwinned angle-resolved photo-emission spectroscopy measurements of FeSe. *New Journal of Physics*, 19(10):103021, 2017. .
  53. M. Yi, H. Pfau, Y. Zhang, Y. He, H. Wu, T. Chen, Z. R. Ye, M. Hashimoto, R. Yu, Q. Si, D.-H. Lee, Pengcheng Dai, Z.-X. Shen, D. H. Lu, and R. J. Birgeneau. Nematic Energy Scale and the Missing Electron Pocket in FeSe. *Phys. Rev. X*, 9:041049, Dec 2019. . URL <https://link.aps.org/doi/10.1103/PhysRevX.9.041049>.
  54. Y. Zhang, M. Yi, Z.-K. Liu, W. Li, J. J. Lee, R. G. Moore, M. Hashimoto, M. Nakajima, H. Eisaki, S.-K. Mo, Z. Hussain, T. P. Devereaux, Z.-X. Shen, and D. H. Lu. Distinctive orbital anisotropy observed in the nematic state of a fese thin film. *Phys. Rev. B*, 94:115153, Sep 2016. . URL <https://link.aps.org/doi/10.1103/PhysRevB.94.115153>.
  55. N. P. Ong. Geometric interpretation of the weak-field Hall conductivity in two-dimensional metals with arbitrary Fermi surface. *Phys. Rev. B*, 43:193, Jan 1991. . URL <https://link.aps.org/doi/10.1103/PhysRevB.43.193>.
  56. Taichi Terashima, Nobuyuki Kurita, Megumi Tomita, Kunihiro Kihou, Chul-Ho Lee, Yasuhide Tomioka, Toshimitsu Ito, Akira Iyo, Hiroshi Eisaki, Tian Liang, Masamichi Nakajima, Shigeyuki Ishida, Shinichi Uchida, Hisatomo Harima, and Shinya Uji. Complete Fermi Surface in  $\text{BaFe}_2\text{As}_2$  Observed via Shubnikov-de Haas Oscillation Measurements on Detwinned Single Crystals. *Phys. Rev. Lett.*, 107:176402, Oct 2011. . URL <http://link.aps.org/doi/10.1103/PhysRevLett.107.176402>.
  57. Andrea Damascelli, Zahid Hussain, and Zhi-Xun Shen. Angle-resolved photoemission studies of the cuprate superconductors. *Rev. Mod. Phys.*, 75:473–541, Apr 2003. . URL <https://link.aps.org/doi/10.1103/RevModPhys.75.473>.
  58. C. H. P. Wen, H. C. Xu, C. Chen, Z. C. Huang, X. Lou, Y. J. Pu, Q. Song, B. P. Xie, Mahmoud Abdel-Hafiez, D. A. Chareev, A. N. Vasiliev, R. Peng, and D. L. Feng. Anomalous correlation effects and unique phase diagram of electron-doped FeSe revealed by photoemission spectroscopy. *Nat. Commun.*, 7:10840, mar 2016. URL <http://dx.doi.org/10.1038/ncomms10840http://10.0.4.14/ncomms10840http://www.nature.com/articles/ncomms10840#supplementary-information>.
  59. Xu Zhang, Zhongpei Feng, Xinjian Wei, Zefeng Lin, Xingyu Jiang, Wei Hu, Zhongxu Wei, Mingyang Qin, Juan Xu, Rui Xiong, Jing Shi, Jie Yuan, Beiyi Zhu, Qihong Chen, and Kui Jin. Enhancement of electron correlations in ion-gated FeSe film by in situ Seebeck and Hall measurements. *Phys. Rev. B*, 103:214505, Jun 2021. . URL <https://link.aps.org/doi/10.1103/PhysRevB.103.214505>.
  60. Andreas Kreisel, Peter J. Hirschfeld, and Brian M. Andersen. On the remarkable superconductivity of fese and its close cousins. *Symmetry*, 12(9), 2020. ISSN 2073-8994. . URL <https://www.mdpi.com/2073-8994/12/9/1402>.
  61. P. O. Sprau, A. Kostin, A. Kreisel, A. E. Böhmer, V. Taufour, P. C. Canfield, S. Mukherjee, P. J. Hirschfeld, B. M. Andersen, and J. C. Séamus Davis. Discovery of Orbital-Selective Cooper Pairing in FeSe. *Science*, 357:75, 2016. URL <https://arxiv.org/abs/1611.02134>.
  62. Chang Liu, Takeshi Kondo, Rafael M. Fernandes, Ari D. Palczewski, Eun Deok Mun, Ni Ni, Alexander N. Thaler, Aaron Bostwick, Eli Rotenberg, Sergey L. Bud'ko, Paul C. Canfield, and Adam Kaminski. Evidence for a Lifshitz transition in electron-doped iron arsenic superconductors at the onset of superconductivity. *Nat. Phys.*, 6:419–423, 2010. . URL <http://dx.doi.org/10.1038/nphys1656>.
  63. N. Shikama, T. Ishikawa, F. Nabeshima, and A. Maeda. Transport properties of  $\text{FeSe}_{1-x}\text{S}_x$  and  $\text{FeSe}_{1-y}\text{Te}_y$  epitaxial thin films under magnetic fields. *Journal of Physics: Conference Series*, 1293:012015, sep 2019. . URL <https://doi.org/10.1088%2F1742-6596%2F1293%2F1%2F012015>.
  64. W. K. Huang, S. Hosoi, M. Čulo, S. Kasahara, Y. Sato, K. Matsuura, Y. Mizukami, M. Berben, N. E. Hussey, H. Kontani, T. Shibauchi, and Y. Matsuda. Non-Fermi liquid transport in the vicinity of the nematic quantum critical point of superconducting  $\text{FeSe}_{1-x}\text{S}_x$ . *Phys. Rev. Research*, 2:033367, Sep 2020. . URL <https://link.aps.org/doi/10.1103/PhysRevResearch.2.033367>.
  65. M. Čulo, M. Berben, Y.-T. Hsu, J. Ayres, R. D. H. Hinlopen, S. Kasahara, Y. Matsuda, T. Shibauchi, and N. E. Hussey. Putative Hall response of the strange metal component in  $\text{FeSe}_{1-x}\text{S}_x$ . *Phys. Rev. Research*, 3:023069, Apr 2021. . URL <https://link.aps.org/doi/10.1103/PhysRevResearch.3.023069>.
  66. Marco Mariani and Lara Benfatto. Resistivity anisotropy from multiorbital Boltzmann equation in nematic FeSe. 2022. . URL <https://arxiv.org/abs/2202.12070>.
  67. Manuel Zingl, Jernej Mravlje, Markus Aichhorn, Olivier Parcollet, and Antoine Georges. Hall coefficient signals orbital differentiation in the Hund's metal  $\text{Sr}_2\text{RuO}_4$ . *npj Quantum Materials*, 4(1):35, 2019. ISSN 2397-4648. . URL <https://doi.org/10.1038/s41535-019-0175-y>.
  68. Ben Lau, Wenlong Wu, and Stephen R. Julian. Revealing an anisotropic electronic scattering rate in the "non-metallic" metal FeCrAs using the Hall effect. *arXiv:2110.09486*, 2021. URL <https://arxiv.org/abs/2110.09486>.
  69. L. Fanfarillo, E. Cappelluti, C. Castellani, and L. Benfatto. Unconventional Hall Effect in Pnictides from Interband Interactions. *Phys. Rev. Lett.*, 109:096402, Aug 2012. . URL <https://link.aps.org/doi/10.1103/PhysRevLett.109.096402>.
  70. R. M. Fernandes, A. V. Chubukov, and J. Schmalian. What drives nematic order in iron-based superconductors? *Nature Physics*, 10:97–104, 2014. .